PHYSICAL REVIEW D **95,** 103005 (2017)

Dark matter interpretation of the *Fermi*-LAT observation toward the Galactic Center

Christopher Karwin,[*] Simona Murgia,[†] and Tim M. P. Tait[‡]
Department of Physics and Astronomy, University of California, Irvine, California 92697, USA

Troy A. Porter[§]
Hansen Experimental Physics Laboratory and Kavli Institute for Particle Astrophysics and Cosmology, Stanford University, Stanford, California 94035, USA

Philip Tanedo[‖]
Department of Physics and Astronomy, University of California, Irvine, California 92697, USA and Department of Physics and Astronomy, University of California, Riverside, California 92521, USA
(Received 5 January 2017; published 5 May 2017)

The center of the Milky Way is predicted to be the brightest region of γ-rays generated by self-annihilating dark matter particles. Excess emission about the Galactic center above predictions made for standard astrophysical processes has been observed in γ-ray data collected by the *Fermi* Large Area Telescope. It is well described by the square of a Navarro, Frenk, and White dark matter density distribution. Although other interpretations for the excess are plausible, the possibility that it arises from annihilating dark matter is valid. In this paper, we characterize the excess emission as annihilating dark matter in the framework of an effective field theory. We consider the possibility that the annihilation process is mediated by either pseudoscalar or vector interactions and constrain the coupling strength of these interactions by fitting to the *Fermi* Large Area Telescope data for energies 1–100 GeV in the $15° \times 15°$ region about the Galactic center using self-consistently derived interstellar emission models and point source lists for the region. The excess persists and its spectral characteristics favor a dark matter particle with a mass in the range approximately from 50 to 190 (10 to 90) GeV and annihilation cross section approximately from 1×10^{-26} to 4×10^{-25} (6×10^{-27} to 2×10^{-25}) cm^3/s for pseudoscalar (vector) interactions. We map these intervals into the corresponding WIMP-neutron scattering cross sections and find that the allowed range lies well below current and projected direct detection constraints for pseudoscalar interactions, but are typically ruled out for vector interactions.

DOI: 10.1103/PhysRevD.95.103005

I. INTRODUCTION

Despite the overwhelming evidence from astrophysics and cosmology that roughly 80% of the matter in our Universe is in the form of dark, nonbaryonic particles, how this so-called dark matter (DM) fits with the Standard Model (SM) of particle physics is currently unknown. Determining the nature of DM is one of the most pressing questions in the physical sciences, and a wide array of experiments are underway which hope to shed light on its identity by observing its interactions with the better understood particles of the SM.

Indirect detection is one of the promising avenues to elucidate the nature of DM. This method attempts to detect and discriminate the SM particles produced by DM particle annihilations (or decays) from those produced by conventional astrophysical processes. γ-rays of $\sim$GeV energies are a particularly effective messenger because they propagate unhindered on galactic scales, and thus can be effectively traced back along the direction of their origin. In recent years, the *Fermi* Large Area Telescope (*Fermi*-LAT) has mapped out the γ-ray sky with the highest sensitivity of space-borne detectors to date, leading to the current best limits on the annihilation cross section for $\sim$100 GeV DM annihilations that result in γ-rays.

Numerical simulations of galaxy formation offer clues as to where DM annihilation is expected to shine the most brightly. The simulations typically predict a large concentration of DM close to the Galactic center (GC), which smoothly falls off with Galactocentric radius. They also predict localized overdensities of DM, some of which correspond to dwarf spheroidal satellite galaxies. Both targets provide complementary regions of interest for DM searches. The DM related emission from the dwarf galaxies is expected to be of lower intensity, but to be relatively free of standard astrophysical backgrounds. Searches for γ-ray emission from dwarf satellites of the

[*]ckarwin@uci.edu
[†]smurgia@uci.edu
[‡]ttait@uci.edu
[§]tporter@stanford.edu
[‖]flip.tanedo@ucr.edu

Milky Way have so far shown no convincing signal of DM annihilation [1–3]. In contrast, the GC is expected to produce a higher intensity annihilation signal. However, the region about the GC is strongly confused because of the intense interstellar emission and numerous discrete sources of γ-rays that are summed along and through the line-of-sight toward the GC. The estimation of these fore/background contributions pose a significant challenge for detection of DM annihilation at the GC.

There seems to be an excess of γ-rays from the direction of the GC, above the expectations from astrophysics. This feature was first observed by Goodenough and Hooper [4,5], and its general features, a spatial morphology remarkably consistent with predictions for a DM annihilation signal and a spectrum that peaks at a few GeV, persist in more recent analyses [6–18]. The *Fermi*-LAT collaboration has released its own analysis [19] of the γ-rays from the direction of the inner galaxy based on specialized interstellar emission models (IEMs) for estimating the fore/background emissions, and enabling the analysis to make the first separation of the γ-ray emission of the $\sim$1 kpc region about the GC from the rest of the Galaxy. Even with these IEMs, which represent the most sophisticated modeling to date, the excess persists. However, its spectral properties are strongly dependent on the assumed IEM, making it challenging to conclusively identify its origin. As a result, it remains unclear whether this signal arises from DM annihilation rather than from a currently unknown contribution from astrophysics such as a large population of millisecond pulsars, cosmic-ray (CR) proton or electron outbursts, additional cosmic ray sources, and/or emission from a stellar overdensity in the Galactic bulge [12,18,20–25]. An interesting development is the use of statistical tools which indicate that GeV photons from the direction of the inner galaxy region show significantly more clustering than would be expected from Poisson noise from smooth components [26–29]. However, it remains difficult with the current models to disentangle whether this feature represents a property of the excess itself, or unmodeled variation in the background components [30].

While it is clearly premature to claim that the GeV excess represents a confirmed signal of DM annihilation, in this paper we extract the properties of the excess under the assumption that it does. We make simultaneous fits to the parameters of generic, realistic particle physics model of DM annihilation together with those defining the broad characterization of the possible fore/backgrounds determined using the methodology of Ref. [19]. As a result, we can compare with the expectations for such models from direct searches for DM and colliders, finding that the null results of those searches play a significant role in shaping the allowed parameter space.

Our work is organized as follows. In Sec. II, we very briefly review the methodology of the *Fermi*-LAT analysis [19] to formulate realistic IEMs, which crucially define the foregrounds and backgrounds as well as the astrophysical contributions from the GC itself. This is followed in Sec. III by a revisitation of some of the most important morphological and spectral features of the signal: its centroid and whether there is evidence for two separate components with distinct morphologies and spectra. In Sec. IV, we define realistic flexible DM models described by effective field theories (EFTs), and perform a maximum likelihood (ML) fit to determine the ranges of their parameters capable of describing the excess together with the IEM parameters. We compare the ML regions of those models to direct and collider searches for DM in Sec. V. Section VI contains our conclusions and outlook.

II. INTERSTELLAR EMISSION MODEL AND ANALYSIS

A. Data

The analysis presented in this paper employs the same data as used by Ref. [19]: front converting events corresponding to the P7REP_CLEAN_V15 selection [31], in the energy range 1–100 GeV, and with zenith angles less than 100°. Exposure maps and the PSF for the pointing history of the observations were produced using the *Fermi*–LAT ScienceTools package (version 09-34-02).[1] Events are selected from approximately 62 months of data, from 08-11-2008 until 10-15-2013. We note that for high-statistics analyses, such as the one presented here, a notable difference is not expected in the results obtained with the P7REP_CLEAN_V15 data processing and those processed using Pass 8 [32]; this is confirmed by several previous analyses [18,28,33].

B. Interstellar emission models

The interstellar emission is the largest contribution to the γ-ray emission toward and through the line-of-sight toward the GC. To separate the contribution by the Galaxy between our location and the inner 1 kpc region about the GC, and that on the other side of the GC, specialized IEMs (four in total) were developed for the Ref. [19] analysis. The methodology employed templates calculated using the well-known GALPROP CR propagation modeling code[2] that were scaled to the data outside of the inner $15° \times 15°$ region about the GC. Under the assumption of Galactocentric azimuthal symmetry, these IEMs were used to estimate the fore/background emission over the $15° \times 15°$ region, enabling the separation. Employing this prescriptive methodology ensures that minimal biases are introduced when fitting to the inner region. In addition, point source lists were developed for each IEM with the properties of the individual point sources obtained in a combined ML fit

[1]Available at http://fermi.gsfc.nasa.gov/ssc/data/analysis

[2]A description of the GALPROP code is available at http://galprop.stanford.edu

over the $15^\circ \times 15^\circ$ region. The construction of each IEM and its associated point-source list/model is a critical improvement over earlier works because the residual emission is strongly dependent on modeling both over the region self-consistently.

The four distinct IEMs from Ref. [19] are labeled as follows:

(i) Pulsars, intensity-scaled
(ii) Pulsars, index-scaled
(iii) OB stars, intensity-scaled
(iv) OB stars, index-scaled

The IEMs differ in the assumed distribution of the sources of CRs as tracing either the distributions of pulsars or OB stars; and in the procedure employed to scale the γ-ray intensity of the fore/background components outside of the $15^\circ \times 15^\circ$ region to the data, either by scaling the normalization of the model templates for intensity-scaled IEMs, or scaling the normalization and spectral index (the latter only for gas-related templates interior to the solar circle) for the index-scaled IEMs. Notably, it was found that the data are compatible with a contribution from γ-rays from DM annihilation, and that the agreement between the data and the model significantly improves for all four IEMs when an additional component with a DM annihilation morphology is included in the fit.

C. Analysis procedure

We employ the procedure developed by the *Fermi*-LAT Collaboration in [19], which performs a ML fit of a model consisting of one of the four IEMs and its corresponding list of point sources to the data in the $15^\circ \times 15^\circ$ region. For each model, we include a DM annihilation contribution (described below) and perform the fit using the *gtlike* package of the *Fermi*-LAT ScienceTools. The results of the fit are the coefficients of the interstellar emission components from within the innermost ~1 kpc, as well as those describing the DM model under consideration. All point sources with a test statistic (defined as in [34]) $TS > 9$ are included in the model. Their fluxes and spectra are determined by iterative fits, with each iteration freeing the spectral parameters for a subset of point sources in order of decreasing TS.

III. MORPHOLOGY AND SPECTRAL CHARACTERISTICS

The DM spatial distribution used in this paper is described in this section. Because [19] tested spatial templates fixed at the position of Sgr A* we investigate the possibility of an offset from this location by refitting the DM spatial distribution and scanning the ML grid about the GC. If a large offset is found, it might challenge a DM interpretation of the excess. For some IEMs the DM spectrum obtained by [19] extended beyond 10 GeV, but a dedicated study of the spatial distribution > 10 GeV was not made; this is also investigated in this section.

A. Dark matter component

The results of numerical simulations for galaxy formation can broadly be described by the Navarro, Frenk, and White (NFW) profile [35]:

$$\rho(r) = \rho_0 \left(\frac{r}{R_s}\right)^{-\gamma} \left(1 + \frac{r}{R_s}\right)^{\gamma-3}. \quad (1)$$

For this analysis, we use a scale radius $R_s = 20$ kpc and ρ_0 corresponding to a local DM density $\rho_\odot = 0.4$ GeV/cm^3. Two values for the inner slope γ of the DM distribution are considered, $\gamma = 1$, 1.2. The more cuspy distribution $\gamma = 1.2$ is motivated by the possibility of halo contraction due to the influence of baryons, which are typically not included in the simulations [36]. The square of the NFW distribution is used as a template for DM annihilation, and we refer to it as the "NFW profile" (for $\gamma = 1$) or "NFW-c" (for $\gamma = 1.2$).

B. NFW centroid

The centroid of the Milky Way DM halo is conventionally centered at the location of Sgr A*. Because a large offset from this location might disfavor a DM interpretation, we verify that the centroid of the excess is sufficiently close. An offset between the centroid of the DM halo and Sgr A* as large as approximately 2° is consistent with numerical DM simulations, with the largest offsets tending to correlate with flatter central profiles [37,38]. An offset in the centroid position was previously reported in [14,39], while other studies of the GC excess have found it to be consistent with Sgr A*.

We investigate the centroid position of the excess by scanning the ML for different locations near Sgr A*, for each of the four IEMs. A power-law with exponential cutoff is employed for the spectral model, following [19]. The scan is performed by making the ML fit following Sec. II with the DM template centered at each point of a grid with spacing 0.2° centered on Sag A*. The results of the scan are shown in Fig. 1, where the color scale shows the $2\Delta \log L$ as a function of Galactic latitude and longitude. The intersections of the dotted grid lines correspond to the points where the likelihood is evaluated. The circle indicates the position of Sgr A*, and the triangle is the most likely position of the centroid for that IEM. We find that the centroid position is offset from Sgr A* for all four IEMs, with the *Pulsars, index-scaled* model displaying the largest offset, both in longitude (0.6°) and latitude (0.2°). The other three models prefer an offset only in longitude (within 0.4° up to the grid accuracy). Based on the scan, Sgr A* is not favored as the location of the NFW centroid for all four IEMs, however its position is roughly consistent with a DM interpretation for the GC excess and imperfections in the

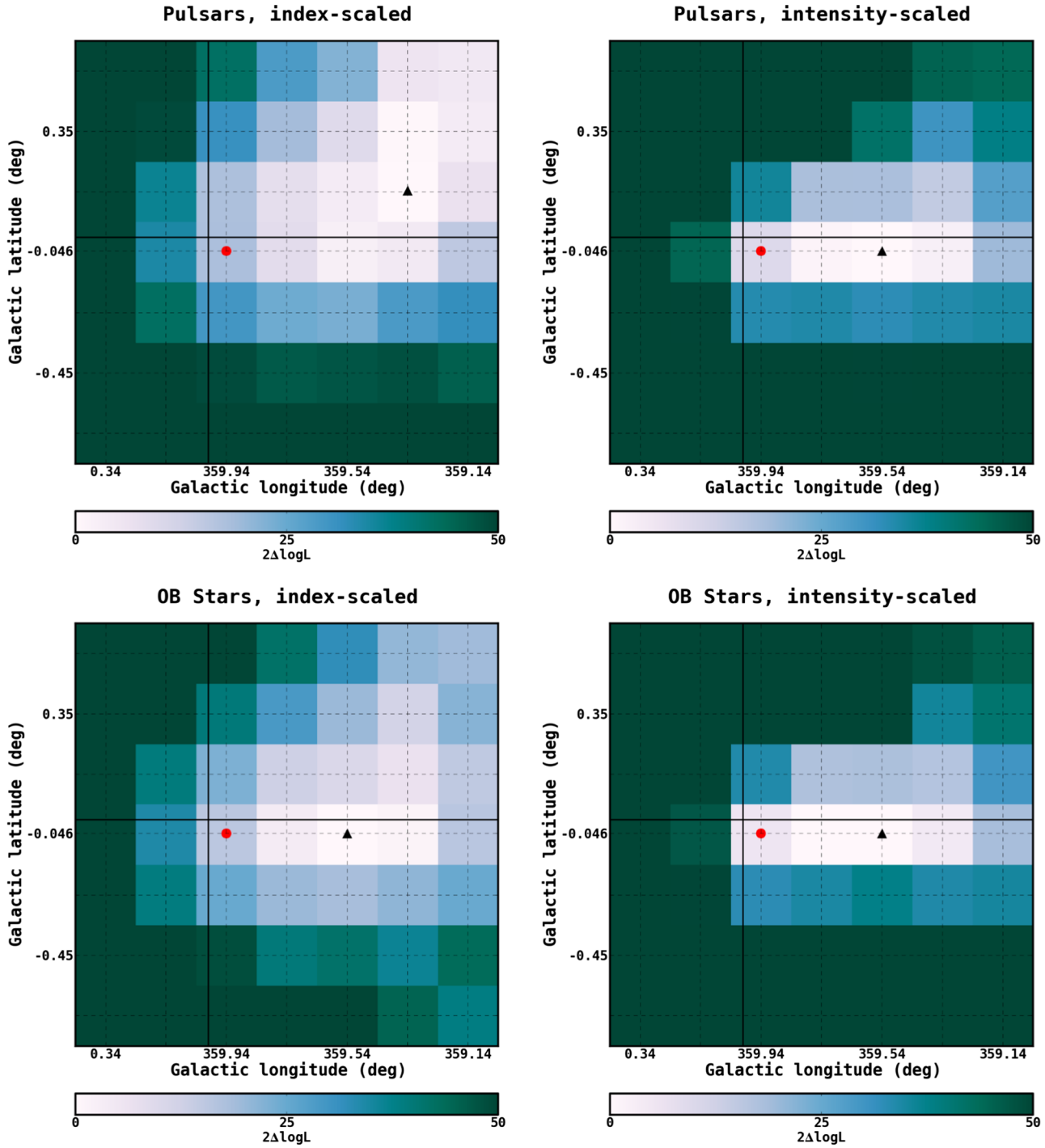

FIG. 1. 2Δ log Likelihood as a function of the centroid position of the NFW template, as described in the text. The results are shown for each of the four considered IEMs, as indicated. The triangle and the circle indicate the position of the ML and of Sag A*, respectively.

IEMs could plausibly introduce an offset. We, therefore, assume for the remainder of this paper that the DM distribution is centered at Sgr A*.

C. Multiple component fit

Whether the high-energy tail (> 10 GeV) of the GeV excess spectrum is related to that at lower energies remains an open issue. In [19], the excess emission above 10 GeV is most prominent in the intensity-scaled IEMs. For the index-scaled variants however, it is largely attributed to interstellar emission (see also [11]). The origin of the > 10 GeV excess has been previously investigated by several studies. In [30], the excess emission above 10 GeV is found to cutoff in the innermost few degrees about the GC (unlike

the excess at a few GeV) and therefore to have a different spatial morphology; secondary emission from unresolved millisecond pulsars is proposed as an interpretation. In [39], the excess emission above 10 GeV is found to have a similar radial profile as the peak emission. Reference [39] also discusses the interplay with the Fermi bubbles, although the bubble morphology close to the Galactic plane is uncertain.

Here we investigate the morphology of the > 10 GeV excess emission present for the Pulsars and OB stars, intensity-scaled IEMs. We perform a ML fit over the 1–100 GeV energy range with two components to model the GC excess: an NFW template; and a second component that has either an NFW, gas, or a two-dimensional Gaussian (with half-width, half maximum of 1°, 2°, 5°, or 10°) morphology. These are the same templates that were employed by [19]. Six template combinations for the two intensity-scaled models are therefore tested. The spectrum for each template is modeled as a power law with an exponential cutoff function. The ML fit is performed iteratively, as described in Sec. II, and the results are shown in Tables I and II for the Pulsars and OB stars and the intensity-scaled IEM, respectively. The NFW + NFW combination is favored over all of the others considered, for both IEMs.

In Fig. 2 the differential fluxes integrated over the $15° \times 15°$ region for the two component fits, along with the fractional residuals, are shown for the Pulsars, intensity-scaled model. The contribution to the flux from each of the two spatial components and the IEM are shown, with the IEM broken down into the contributions from inverse Compton (IC), π^0 emission from the inner $\sim$1 kpc ("ring 1" in the legend), and from the point sources. For each of the six combinations we consider, the low energy excess is better described by an NFW morphology. The more peaked two-dimensional Gaussian templates (1° and 2°) have spectra that peak in the few GeV energy range and cutoff at higher energies. Note that their contribution is always well below the contribution assigned to the NFW template. On the other hand, the spectra for the broader two-dimensional Gaussian templates (5° and 10°) are more prominent at higher energies, suggesting that the high-energy tail of the GeV excess is consistent with an extended component in the region. The NFW morphology, which is peaked towards the GC and broadly extended in the region, is better suited to model the excess emission over the full energy range compared to the other options we have considered. However, due to the limitations of the IEMs together with the limited statistics at the higher energies, it is difficult to conclude decisively whether or not the high-energy tail is a true feature of the GC excess. Given the current preference for a single NFW morphology for both low and high energy components, we include the full energy range when comparing with the DM scenarios in Sec. IV below.

TABLE I. Results for the multiple component fit for the Pulsars, intensity-scaled IEM.

Fit components (1 + 2)	log L	2Δ log L
NFW + NFW	−82870	844
NFW + Gas template	−82942	700
NFW + 1° Gauss	−82968	648
NFW + 2° Gauss	−82932	720
NFW + 5° Gauss	−82951	682
NFW + 10° Gauss	−82950	684
NFW only	−82990	604
Null hypothesis	−83292	–

TABLE II. Results for the multiple component fit for the OB stars, intensity-scaled IEM.

Fit components (1 + 2)	log L	2Δ log L
NFW + NFW	−82972	914
NFW + Gas template	−83068	722
NFW + 1° Gauss	−83096	666
NFW + 2° Gauss	−83065	728
NFW + 5° Gauss	−83147	564
NFW + 10° Gauss	−83111	636
NFW only	−83099	660
Null hypothesis	−83429	–

IV. DARK MATTER INTERPRETATION

In this section, we fit the parameters of particle physics models of DM, together with the parameters describing the fore/backgrounds, extracting a comprehensive DM interpretation of the GC excess. As described in more detail below, we employ a parameterization of the DM particle physics model which allows for distinct annihilation rates into up-type quarks, down-type quarks, and leptons. Our parametrization has more flexibility than the often-considered annihilation into a single channel of SM particles and, in this sense, is better able to capture a wider array of realistic particle physics models for DM annihilation than those typically used in indirect searches.

A. EFT description of dark matter interactions

We consider two representative EFTs that describe the DM interactions with the SM fermions. These theories form part of a universal set of operators to which any theory of DM flows at low energies, well below the masses of the particles responsible for communicating between the SM and the dark matter [40–45]. Such models have previously been considered to describe the GC excess [46,47]. More generalized constructions are employed here, and their parameters are fit together with the IEM parameters as described in Sec. II. Of course, models with light mediators are also interesting, and worthy of investigation in their

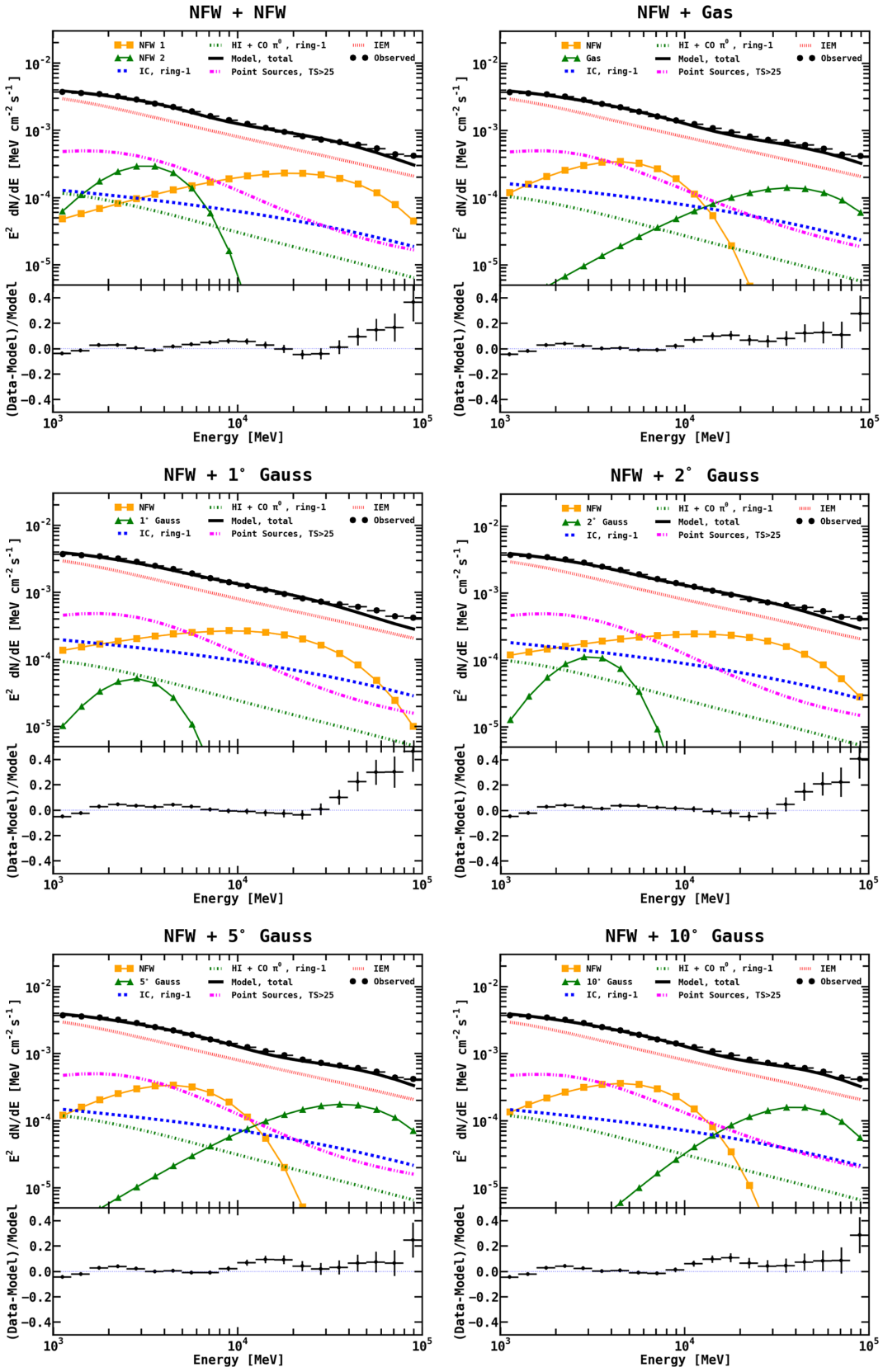

FIG. 2. Differential fluxes (broken down into components, as indicated) integrated over the $15° \times 15°$ region for the two component fits, along with their fractional residuals, for the Pulsars, intensity-scaled IEM.

own right [48–56]. We leave exploration of such theories for future work.

Both of our considered EFTs are chosen such that they mediate s-wave (velocity-unsuppressed) annihilation, because a p-wave annihilation mechanism would require such strong interactions to overcome the innate $v^2 \sim 10^{-4}$ suppression that it is likely to already be ruled out by direct and/or collider searches. We further restrict them to follow the principle of minimal flavor violation (MFV) [57], such that the most stringent constraints from flavor-violating observables are mitigated by small Yukawa interactions. We consider models containing either pseudoscalar or vector Lorentz structures described by Lagrangians $\mathcal{L}_{\rm ps}$ and $\mathcal{L}_{\rm vec}$ (respectively, in the fermion mass basis),

$$\mathcal{L}_{\rm ps} = \bar{\chi}\gamma_5\chi \times \sum_i \left\{ \frac{m_{u_i}}{\Lambda_u^3}\bar{u}_i\gamma_5 u_i + \frac{m_{d_i}}{\Lambda_d^3}\bar{d}_i\gamma_5 d_i + \frac{m_{\ell_i}}{\Lambda_\ell^3}\bar{\ell}_i\gamma_5\ell_i \right\}, \quad (2)$$

$$\mathcal{L}_{\rm vec} = \bar{\chi}\gamma^\mu\chi \times \sum_i \left\{ \frac{1}{\Lambda_u^2}\bar{u}_i\gamma_\mu u_i + \frac{1}{\Lambda_d^2}\bar{d}_i\gamma_\mu d_i + \frac{1}{\Lambda_\ell^2}\bar{\ell}_i\gamma_\mu\ell_i \right\}, \quad (3)$$

where $i = 1, 2, 3$ is the sum over fermion flavor with the indicated relative weighting of m_{f_i} (1) for the pseudoscalar (vector) interaction types, as dictated by the leading terms consistent with MFV. The $\Lambda_{u,d,\ell}$ are parameters with dimensions of energy which specify the separate interaction strengths between the DM and up-type quarks, down-type quarks, and charged leptons. Together with the DM mass, m_χ, these coefficients specify the point in parameter space for the DM model. They represent generalizations (in that they allow the couplings of up-type and down-type quarks and leptons to vary independently) of the commonly considered interactions D4 and D5 used in DM searches via direct detection and at colliders [43].

B. γ-ray flux from dark matter annihilation

The interactions in both the pseudoscalar and vector models defined in Eqs. (2), (3) lead to cross sections for a pair of DM particles to annihilate $\chi\bar{\chi} \to f\bar{f}$ (where f is any SM fermion):

$$\langle\sigma_f v\rangle_{\rm ps} = \frac{N_f m_f^2 m_\chi^2}{\Lambda_f^6\pi}\sqrt{1-\frac{m_f^2}{m_\chi^2}} + \mathcal{O}(v^2), \quad (4)$$

$$\langle\sigma_f v\rangle_{\rm vec} = \frac{N_f(2m_\chi^2+m_f^2)}{\Lambda_f^4\pi}\sqrt{1-\frac{m_f^2}{m_\chi^2}} + \mathcal{O}(v^2), \quad (5)$$

where $\langle\cdot\rangle$ indicates averaging over the DM velocity profile, $N_f = 3$ (1) for quarks (leptons) counts their color degrees of freedom, and Λ_f is the appropriate $\Lambda_{u,d,\ell}$ for the fermion under consideration. The inclusive cross section for annihilation into up-type quarks, down-type quarks, and charged leptons is the sum of the individual cross sections for all three flavors of each fermion type, and the total cross section $\langle\sigma v\rangle$ is the sum of the three inclusive cross sections. In presenting results, we typically trade the three parameters $\Lambda_{u,d,\ell}$ for $\langle\sigma v\rangle$ and the fractional cross sections f_u, f_d, and f_ℓ (with $f_u + f_d + f_\ell = 1$). It is easy to map these back into the $\Lambda_{u,d,\ell}$ parameters using the appropriate single channel cross section from Eqs. (4) and (5).

The γ-ray intensity and spectrum from DM annihilation is constructed by summing over all of the annihilation channels:

$$\frac{dN_\gamma}{dE} = \sum_f \frac{\langle\sigma_f v\rangle}{4\pi\eta m_\chi^2}\frac{dN_\gamma^f}{dE} \times \int_{\Delta\Omega} d\Omega' \int_{\rm los} ds\rho^2(r(s,\psi)), \quad (6)$$

where dN_γ^f/dE is the number of γ rays per annihilation into the $f\bar{f}$ channel, generated from the PPPC 4 DM ID package [58] based on fits to Pythia 8.1 [59], and $\eta = 2(4)$ for Majorana (Dirac) DM. The integral is the J-factor, obtained by integrating the DM density $\rho^2(\mathbf{x})$ corresponding to either an NFW or NFW-c distribution, Eq. (1), over the line of sight (los) in direction ψ.

To determine the preferred DM model parameters for each IEM, we fix the DM mass in the range from 10–250 GeV in 10 GeV increments. For each mass hypothesis the analysis procedure of Sec. II determines the fitted values of the DM model parameters f_u, f_d, and f_ℓ, along with the coefficients of the interstellar emission components from within the innermost ∼1 kpc and point sources, as usual. We repeat this scan for both NFW and NFW-c annihilation morphologies and for both the pseudoscalar and vector models described above. We find that the DM component is detected with high statistical significance for all IEMs, and for pseudoscalar as well as vector interactions. The likelihood values for pseudoscalar interactions are summarized in Table III.

TABLE III. Likelihood (log L) values for all IEMs for pseudoscalar interactions and for NFW and NFW-c templates.

IEM	log L (null hypothesis)	log L (NFW)	log L (NFW-c)
Pulsars, index-scaled	−82926	−82738	−82739
Pulsars, intensity-scaled	−83292	−82965	−82956
OB stars, index-scaled	−82993	−82779	−82806
OB stars, intensity-scaled	−83429	−83081	−83117

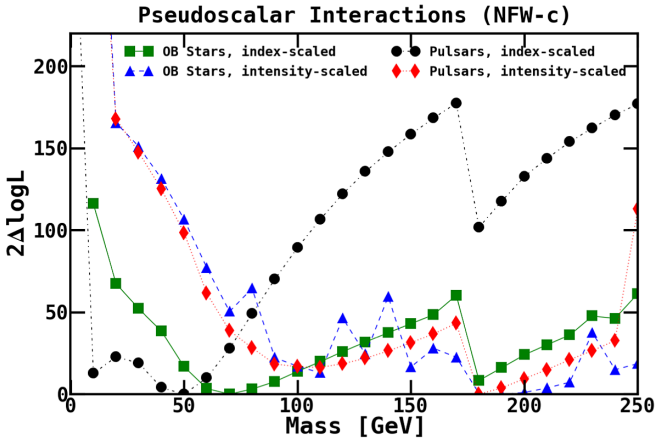

FIG. 3. Likelihood ($2\Delta \log L$) as a function of the DM mass for the pseudoscalar interaction model with NFW-c morphology. Results are shown for all four IEMs, as indicated.

C. Results for pseudoscalar interactions

In Fig. 3, we display the likelihood profile as a function of the DM mass for each of the IEMs for the NFW-c annihilation morphology. The results for the NFW morphology are qualitatively similar. Each of the four IEMs shows a clear preference for particular DM masses, but there is considerable variation between them, with the index-scaled models favoring a mass around ∼50 GeV, while the intensity-scaled models favor higher masses ∼200 GeV. The results are consistent with the results obtained by [19], where the spectrum of the GC excess for the index-scaled IEMs displays a lower energy cutoff compared to the intensity-scaled IEMs. The spectra we consider here correspond to motivated DM scenarios, in contrast with the simpler assumptions made for the spectral model by [19].

In Fig. 4, we present the ML fractions into the three annihilation channels as a function of the DM mass, for each of the IEMs with the NFW-c annihilation morphology. These also vary considerably from one IEM to another, and are characterized by one channel or another typically dominating at any given DM mass hypothesis: charged leptons at lower masses ∼10–20 GeV; down-type quarks in the range ∼50–170 GeV; and up-type quarks above 180 GeV and at lower masses ∼20–40 GeV. The lepton flux declines steeply above ∼20 GeV, and its contribution to the flux is smaller for the index-scaled models (*Pulsars* in particular) compared to the intensity-scaled ones. This reflects in part the lower energy cutoff of

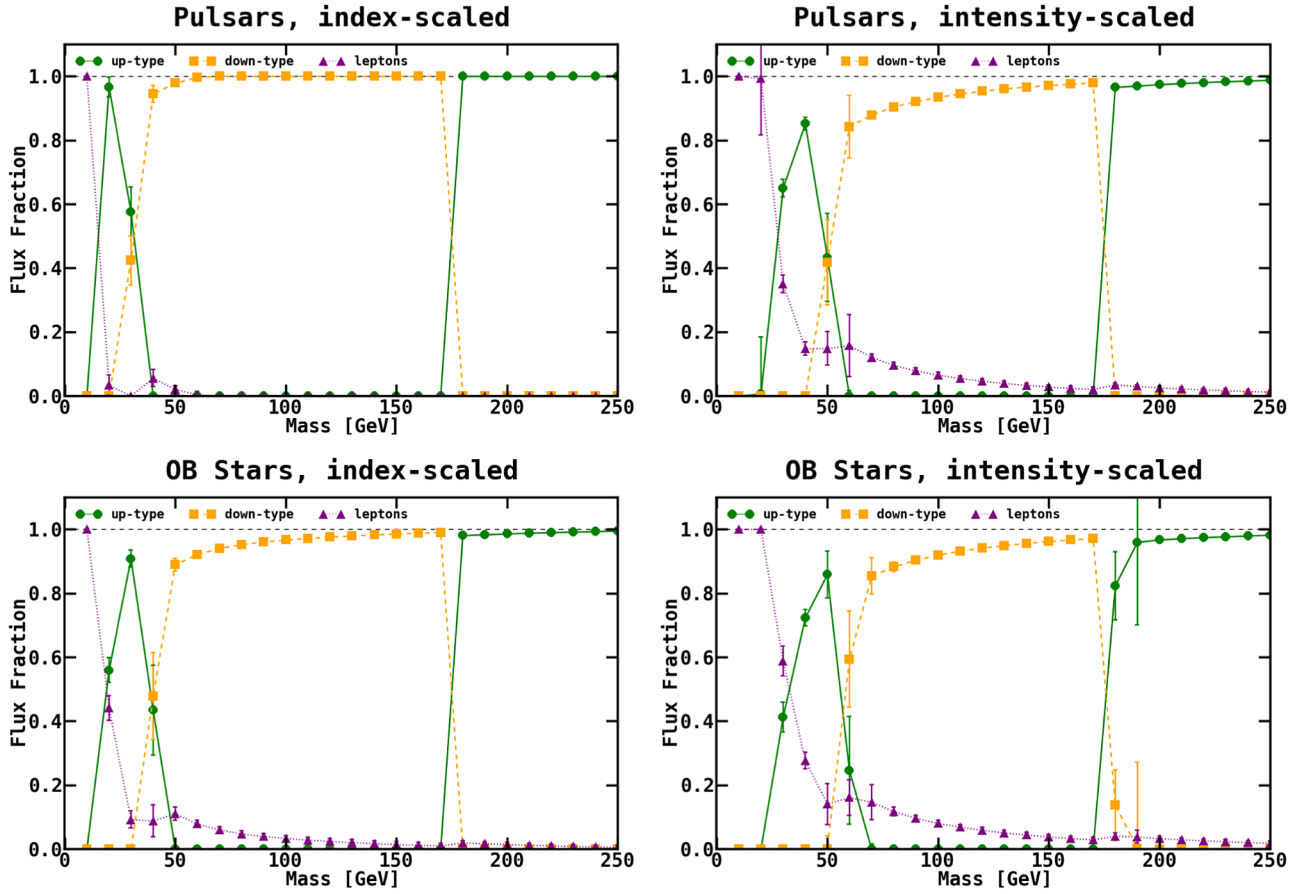

FIG. 4. Flux fraction for annihilation into up-type quarks, down-type quarks, and charged leptons, for the pseudoscalar interaction model with NFW-c morphology. Results are shown for all four IEMs, as indicated.

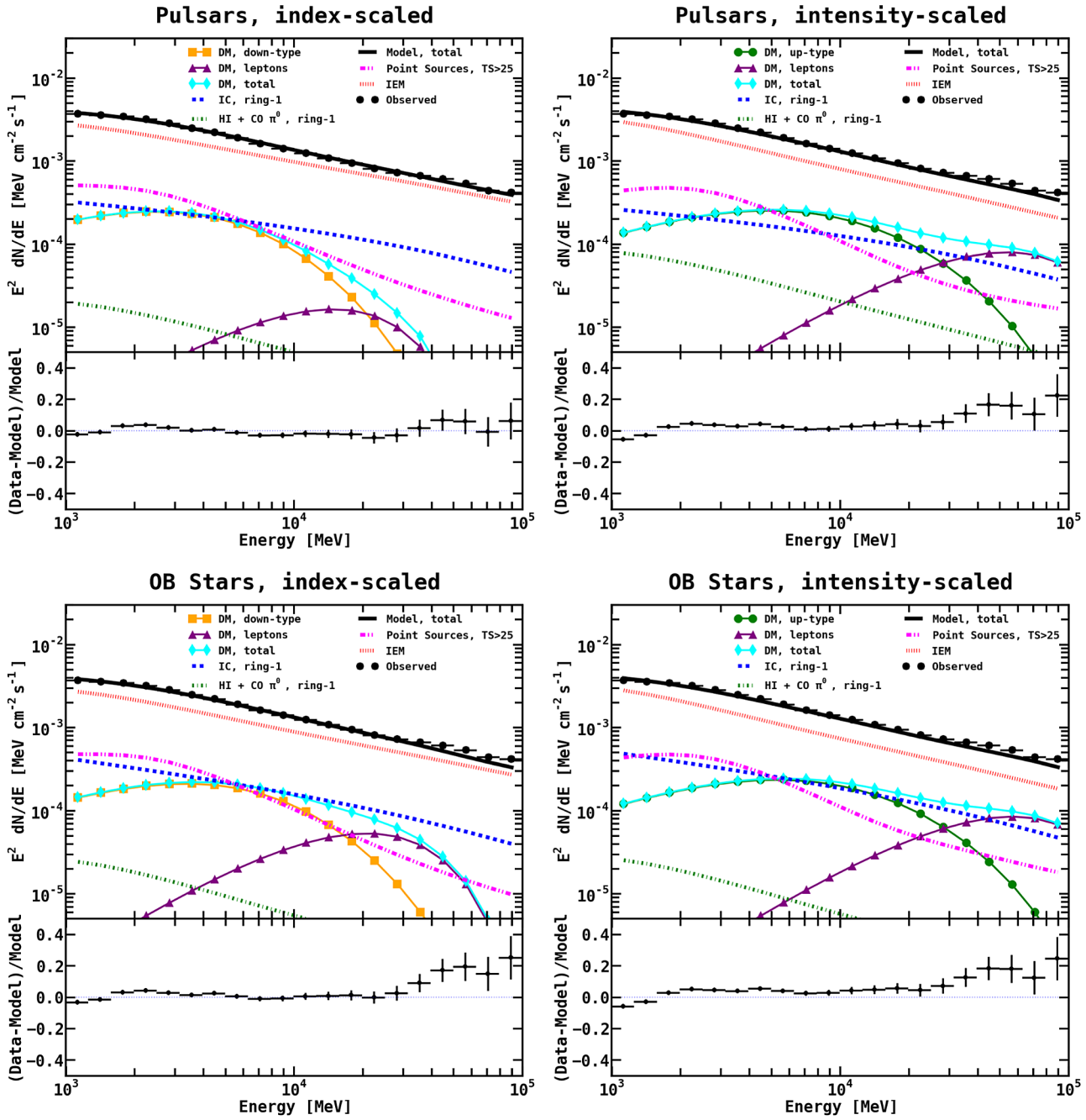

FIG. 5. Differential fluxes (broken down into components, as indicated) integrated over the $15° \times 15°$ region and corresponding fractional residuals for pseudoscalar interactions and for the four IEMs.

the GC excess spectrum for the index-scaled models and the harder γ-ray spectra produced by charged leptons compared to quarks. Also of note is the sharp transition from annihilation into down-type quarks to up-type quarks at the top mass threshold, ~175 GeV. This follows because the pseudoscalar model annihilations are dominated by the heaviest quark kinematically accessible, and top quarks produced close to at rest decay into ~60 GeV bottom quarks, corresponding to the ML region at $m_\chi \sim 50$ GeV.

The best-fit DM mass for the Pulsars (OB stars) index-scaled IEM is 50^{+10}_{-10} GeV (70^{+15}_{-10} GeV), and in both cases annihilation is predominantly into bottom quarks.[3] These results are compatible with the findings of previous studies [60,61] interpreting the spectrum of the excess as presented in Ref. [19]. The intensity-scaled IEMs favor higher DM

[3]The grid spacing is taken into account in the quoted uncertainties on the DM mass.

masses, 180^{+15}_{-5} and 190^{+25}_{-15} GeV, for the Pulsars and OB stars variants, respectively, and primarily favor annihilation into top quarks. We note that the likelihood profile for the OB stars, intensity-scaled IEM is rather flat around the minimum, which yields a higher uncertainty in the best-fit DM mass, compared to the other IEMs. The uncertainties on the flux fractions into up-type and down-type quarks in this mass range are also somewhat larger.

The differential fluxes for the ML model (and the data points) are shown for each IEM in Fig. 5. Individual model components are displayed separately, including the contribution to the DM flux from each annihilation final state, as well as their sum. The contribution from each DM annihilation channel illustrates the fact that the integrated DM flux originates primarily from annihilations into quarks with the harder spectrum from annihilation into leptons becoming important at higher energies, particularly for the intensity-scaled IEMs. The γ-ray emission correlated with gas from the innermost $\sim$1 kpc is subdominant in the region. Fig. 5 also shows the fractional residuals as a function of energy. The agreement between data and model is at the level of a few % or better up to $\sim$30 GeV for all IEMs, and is generally worse at higher energies for all but the Pulsars, index-scaled IEM. It is plausible that the energy cutoff at the DM mass in the annihilation spectrum limits its ability to describe the excess at the higher energies while simultaneously providing a good fit to the data in the few GeV range. We note that the fractional residuals based on

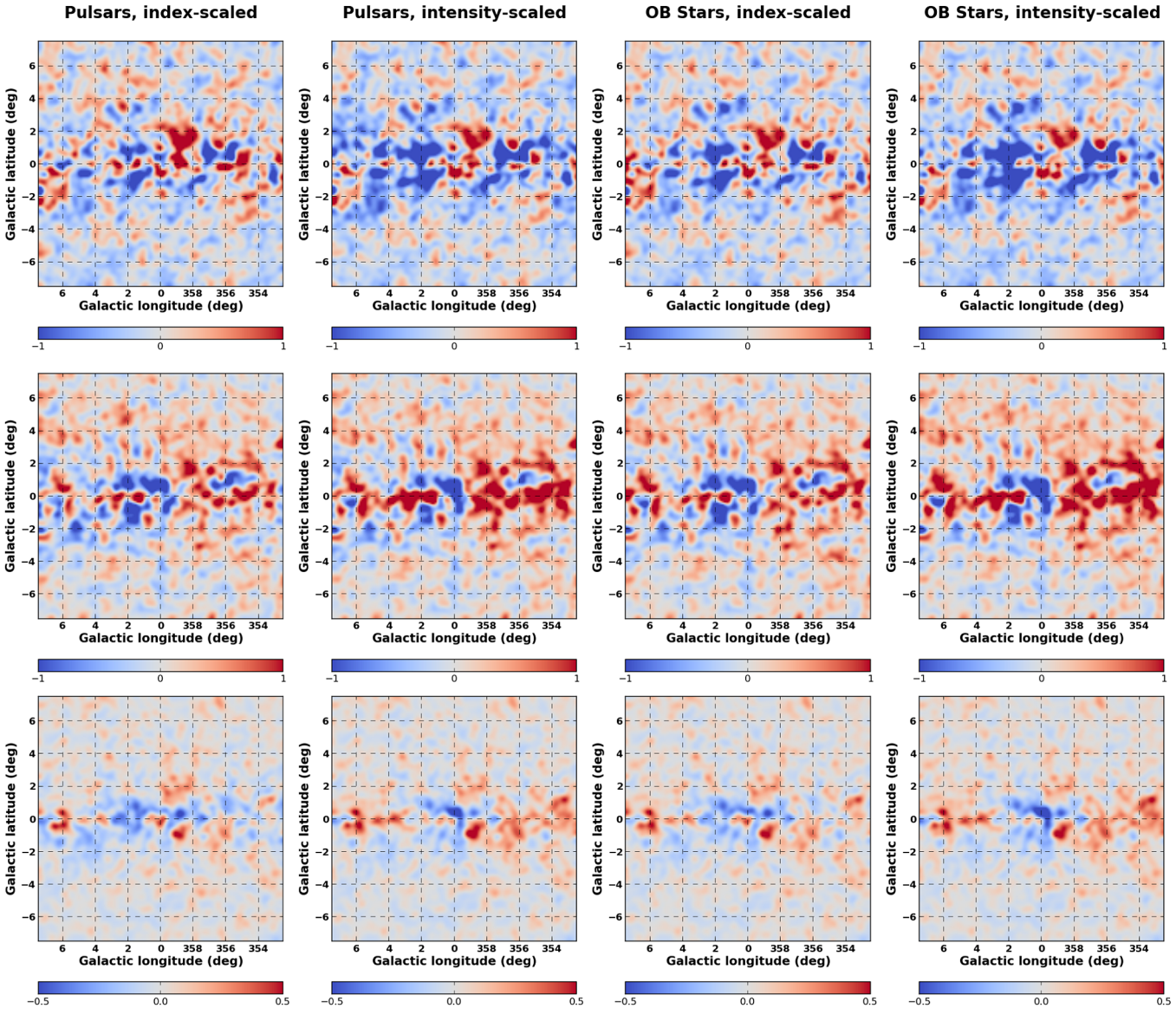

FIG. 6. Residuals (data-model) in three energy bands, for the four IEMs. The rows correspond to the range 1–1.6 GeV (top), 1.6–10 GeV (center), and 10–100 GeV (bottom). The columns, going from left to right are Pulsars, index-scaled; Pulsars, intensity-scaled; OB stars, index-scaled; OB stars, intensity-scaled.

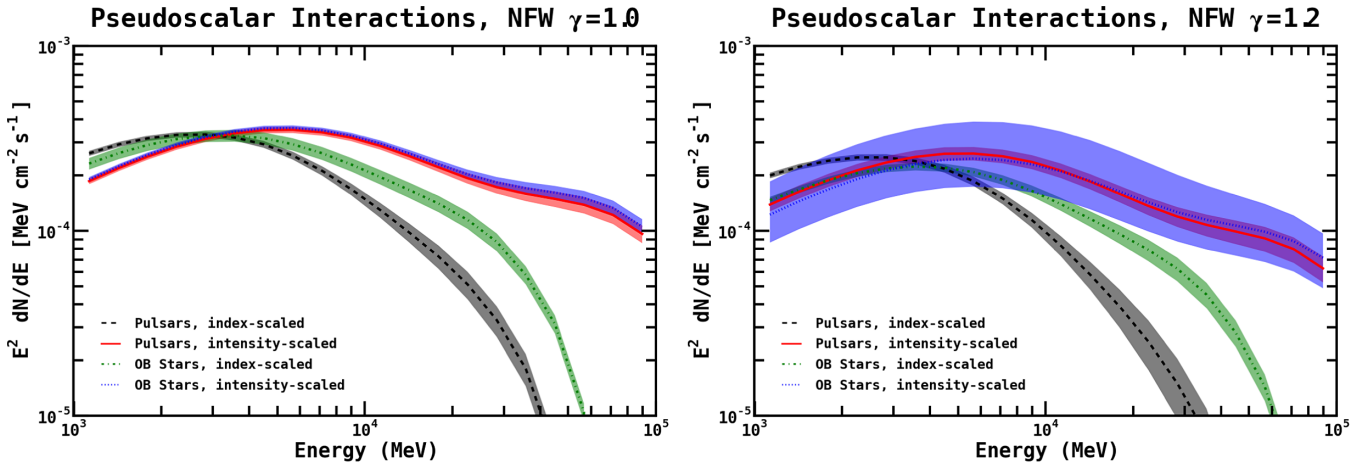

FIG. 7. Differential flux integrated over the 15° × 15° region for the DM component for pseudoscalar interactions, NFW and NFW-c profiles, for all four IEMs, as indicated. The bands represent the fit uncertainties on the normalization.

realistic DM models including up-type, down-type, and lepton final states generally improve (for the same number of free parameters) over the results in [19] based on a power law with exponential cutoff spectrum.

Residual count (data-model) maps are shown in Fig. 6 for the energy bands 1–1.6, 1.6–10, and 10–100 GeV, for each IEM. Structured excesses and deficits remain that may be attributed to imperfect modeling of the interstellar emission. Because of this, we do not rule out the DM models corresponding to IEMs with larger fractional residuals as these discrepancies might be explained by limitations in the IEMs. There is better agreement with the data when the DM spectrum is modeled with power law functions in 10 independent energy bins as done in [19]; perhaps unsurprising given the larger number of free parameters for the spectral model.

The differential flux from the total DM annihilation component for both profiles (NFW, NFW-c) and all four IEMs are summarized in Fig. 7. The bands represent the 1σ fit uncertainty on the flux summing the up-type, down-type, and lepton final states. For the index-scaled variants of the IEMs, the spectrum peaks at a few GeV, while for the intensity-scaled counterparts the peak shifts to higher energies. This is consistent with the requirement that the high energy tail in the spectrum for the intensity-scaled IEMs, predominantly from annihilations into leptons, has to cutoff at the same energy (corresponding to the DM mass) as the contribution to the flux from annihilations into up-type and down-type quarks, which dominate the DM flux at lower energies. Finally, we note that the flux for NFW-c profile is smaller compared to the NFW profile. As a consequence, a simple rescaling based on J-factors when comparing fit results obtained with different profiles is not accurate, as the flux assigned to the DM component has a dependence on the specific morphology.

We translate the DM template flux for each IEM into the inclusive annihilation cross section, with the results shown in Fig. 8. Also shown for comparison is the $\langle\sigma v\rangle$ predicting saturation the measured DM relic density for a standard cosmology [62]. The results for the index-scaled models are comparable to those found in most of the earlier studies of the GeV excess [5,7–16,18]. The intensity-scaled models however are consistent with larger DM masses and cross sections, as first discussed in [60], based on the spectra from [19].

D. Results for vector interactions

The analysis for the vector-type DM interactions proceeds very similarly to the analysis of the pseudoscalar interactions described above. For each IEM and both NFW

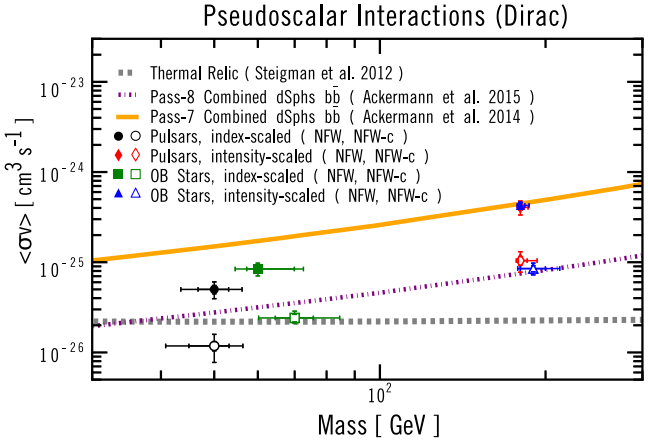

FIG. 8. Masses and cross sections for pseudoscalar interaction models (including one and two sigma uncertainties as the tick marks) for NFW and NFW-c DM profiles, and the four IEMs, as indicated. Also shown are the cross sections saturating the standard thermal relic density (grey dashed line) and the *Fermi*-LAT 95% C.L. bounds from dwarf spheroidal galaxies, for Pass-7 as well as Pass-8 data, assuming 100% annihilation into $b\bar{b}$.

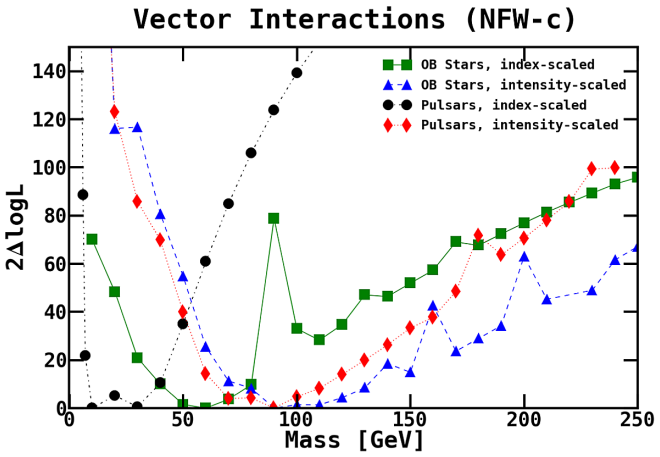

FIG. 9. Likelihood ($2\Delta \log L$) as a function of the DM mass for the vector interaction model with NFW-c morphology. Results are shown for all four IEMs, as indicated.

and NFW-c morphologies, the DM mass is scanned and the couplings to up-type quarks, down-type quarks, and charged leptons is fit. The results are presented in Figs. 9 and 10, respectively, for each IEM with the NFW-c profile (the results for the NFW profile are qualitatively similar.) Similarly to pseudoscalar interactions, lower DM masses are favored by the index-scaled IEMs, compared to the intensity-scaled. However, in general, lower DM masses are favored for the vector interaction models than for the pseudoscalar ones for the same IEM. In addition, because the coupling to SM fermions is assumed to be flavor universal for the vector interaction model, there is no sharp transition in behavior at the top quark mass. For the Pulsars, index-scaled IEM, there are two close-to-degenerate minima in the likelihood profile, with the lower mass dominated by annihilations into leptons.[4] The fitted values of $\langle \sigma v \rangle$ and the DM mass for each of the IEMs and DM profiles are shown in Fig. 11.

V. COMPARISON WITH OTHER SEARCHES

As seen in Secs. IV C and IV D, DM interpretations of the GC excess cover a broad range of masses ($\sim$10–200 GeV) and $\langle \sigma v \rangle$, depending on the IEM, DM profile, and interaction type. One crucial avenue toward exploring a DM hypothesis for the excess is to compare the regions of parameter space best describing the excess with the results from other searches for DM. Null results of such searches can sharpen the target parameter space or even exclude candidate explanations, whereas positive results could strengthen a DM interpretation of the excess and better define the characteristics of candidate models.

A. Indirect searches

For masses in the range 10–200 GeV, the strongest constraints from indirect detection are generally from *Fermi*-LAT observations of dwarf spheroidal galaxies [1–3]. These limits appear to constrain the region relevant for explanations of the GC excess,[5] but are derived from less theoretically motivated DM annihilation models where the DM annihilates into one species of SM fermion at a time. As such, they do not precisely apply to the models considered here, although similar conclusions are likely. The bound based on the assumption of 100% annihilation into $b\bar{b}$, corrected to account for Dirac (rather than Majorana) DM particles, is shown on Figs. 8 and 11 for reference. The dwarf spheroidal bounds for annihilations into leptons are not displayed in these figures. Although they would, in principle be more pertinent to constrain our low mass, vector interaction results, they are still not adequate as the final state channel we consider here is an equal weight mixture of e^+e^-, $\mu^+\mu^-$, $\tau^+\tau^-$ and therefore not directly comparable.

The limitations in the IEMs, modeling uncertainties in the dwarf halos [66–69], modifications to the particle physics model for DM [70], and large uncertainties in the J-factor for the GC [71], all widen the relative uncertainties when confronting the parameters describing the GC excess with the limits from observations of dwarf spheroidal galaxies. Because of this, care must be taken when contrasting these limits with a DM interpretation of the GC excess.

The particle physics models under consideration also lead to annihilations producing antimatter, such as positrons or antiprotons. Positrons in particular show excess production compared to naive expectations [72,73], leading to limits which do not significantly constrain the parameters for the GC excess [74]. Recently, Ref. [75] (see also [76]) performed a detailed analysis of the antiproton spectrum measured by AMS-02 [77], and also found an indication for an excess component roughly consistent with the parameter space describing a DM interpretation of the GC excess (see [78] for a less optimistic view). The interpretation of CR antimatter measurements is complicated by propagation, energy losses, and other modeling uncertainties related to particle fragmentation, as well as the spatial distribution of astrophysical sources. Consequently, the interpretation of these data in terms of DM is unclear.

B. Direct searches

Coupling to quarks implies coupling to hadrons, and thus is bounded from direct searches for DM scattering with heavy nuclei. Models with pseudoscalar interactions map

[4]For annihilations into leptons, secondary γ-ray emission via IC processes is neglected. Note that for DM masses $\lesssim$10 GeV, IC photons are mainly produced at energies < 1 GeV [63,64].

[5]Note that an excess from the Reticulum II dwarf galaxy has been claimed [65]. We find that our interpretation of the GC excess is not in conflict with this observation.

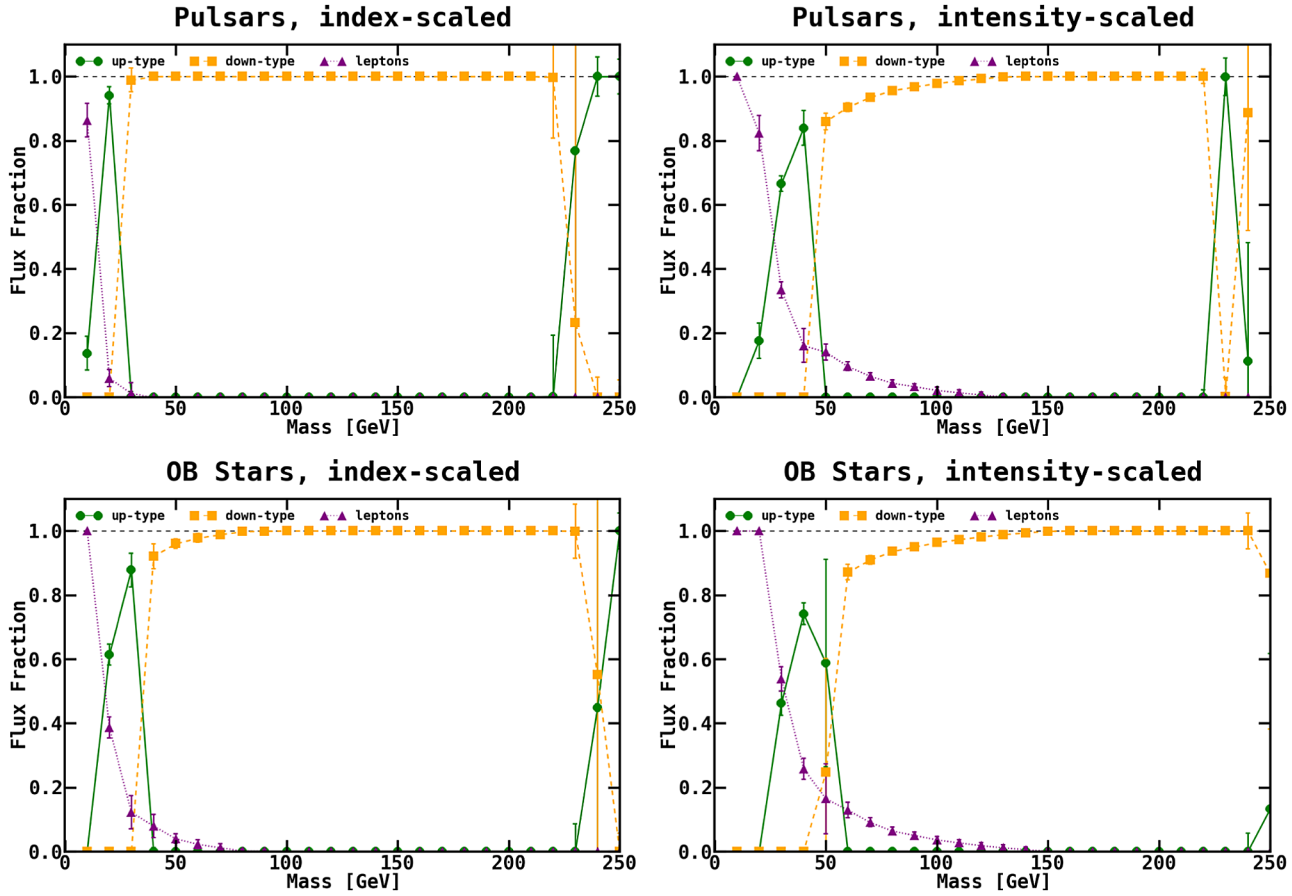

FIG. 10. Flux fraction for annihilation into up-type quarks, down-type quarks, and charged leptons, for the vector interaction model with NFW-c morphology. Results are shown for all four IEMs, as indicated.

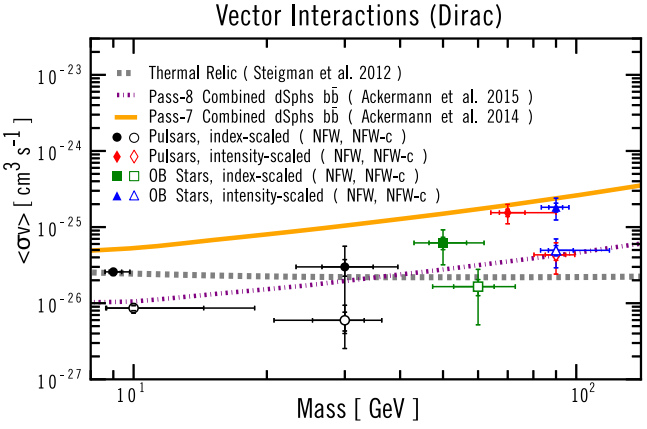

FIG. 11. Masses and cross sections for vector interaction models (including one and two sigma uncertainties) for NFW and NFW-c DM profiles, and the four IEMs, as indicated. Also shown are the cross sections saturating the standard thermal relic, density (grey dashed line) and the *Fermi*-LAT 95% C.L. bounds from dwarf spheroidal galaxies, for Pass-7 as well as Pass-8 data, assuming 100% annihilation into $b\bar{b}$.

onto a scattering cross section which is both suppressed by the small velocities of DM in the Galactic halo and are also spin-dependent. As a result, the expectation is that the null results of direct searches yield mild constraints which are roughly v^2 smaller than the constraints on $\sigma_{\rm SD}$ quoted by e.g. IceCube [79]. In contrast, vector interactions lead to velocity-unsuppressed spin-independent scattering and are strongly constrained by direct searches. For the vector models, which contribute to the spin-independent cross section $\sigma_{\rm SI}$, we follow the usual convention mapping onto this quantity defined at zero relative velocity. For pseudoscalar interactions, we compute the integrated cross section for DM scattering with a nucleon by integrating over the recoil energy of the nucleus and the velocity of the DM, which we assume follows a Maxwellian distribution, using techniques developed in [80–83], (specifically using the code presented in Ref. [82]). This integrated cross section should be distinguished from usual spin-dependent cross section $\sigma_{\rm SD}$, defined at zero velocity scattering, and is a more appropriate measure of scattering which is strongly velocity dependent.

In Figs. 12 and 13, we show the ML points for the pseudoscalar and vector models mapped into the

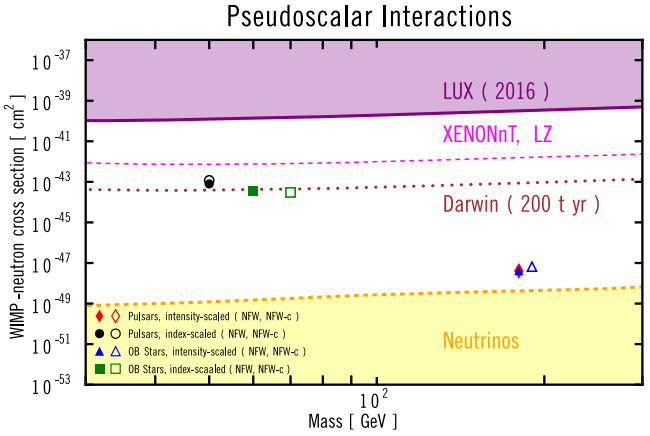

FIG. 12. ML points for the pseudoscalar models, for each IEM and profile considered, as indicated, mapped into the plane of the DM mass and the integrated cross section, as described in the text. Also shown are current constraints from LUX (upper shaded region) and projections from XENONnT, LZ, and Darwin (dashed and dotted lines). The lower shaded region indicates the neutrino floor.

WIMP-neutron spin-dependent integrated cross section, respectively, for each IEM and both NFW and NFW-c. For comparison, the limits from the LUX search for DM scattering with Xenon are presented [84], also mapped into $\sigma_{\rm SI}$ or the integrated cross section for spin-dependent scattering with neutrons. For the vector models, the limits from LUX easily exclude all of the ML points except for the point with dark matter masses around 10 GeV which annihilates predominantly into leptons for the Pulsars, index-scaled IEM with NFW-c profile, which has sufficiently small coupling to quarks that the scattering with nuclei is highly suppressed. For the pseudoscalar models, the predictions for the ML points lie well below the

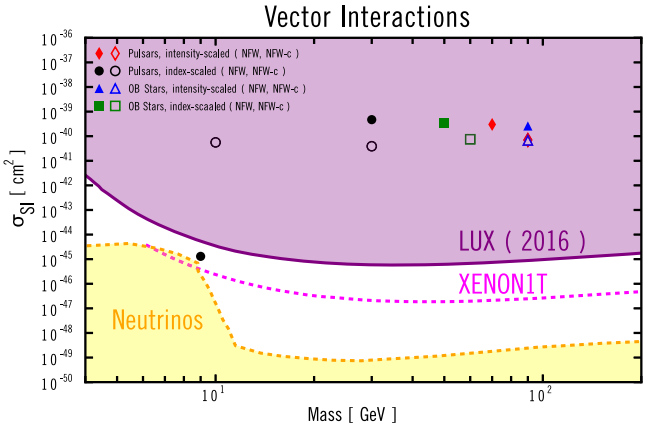

FIG. 13. ML points for the vector models, for each IEM and profile considered, as indicated, mapped into the plane of the DM mass and $\sigma_{\rm SI}$, as described in the text. Also shown are current constraints from LUX (upper shaded region) and projections from XENON1T (dashed line). The lower shaded region indicates the neutrino floor.

LUX bounds, with the lower mass points potentially probed long-term by Darwin [85], while the higher mass points are slightly above the neutrino floor [86] and out of the reach of these experiments. These results illustrate the importance of the IEM modeling and its influence on characterization of the putative signal, which can lead to drastic differences in the expectations from complementary searches.

C. Collider searches

Searches at the Large Hadron Collider (LHC) are more model dependent and can be classified based on the masses and couplings of the particles mediating the interaction. When such particles are heavy compared to the typical collider energies, they can be described by the same EFTs employed in this paper. The results of searches in this regime are typically not competitive with direct searches except at masses far below those of interest to describe the GC excess [87,88]. For lighter mediating particles, the limits depend sensitively on the specific couplings to the DM as well as to the SM fermions. In particular, for values of the cross sections similar to what has been found in past characterizations of the GeV excess, cases where a pseudoscalar mediator's coupling to DM is significantly weaker than the coupling to quarks are mildly constrained by LHC data, and the opposite limit is essentially unconstrained [89]. Given the wide range of parameter space (which is even larger for the specialized IEM analysis considered here), it seems possible that the LHC could eventually hope to observe an excess consistent with a pseudoscalar mediator interpretation if parameters are favorable. Similar remarks apply to the vector mediator models, although all but the Pulsars, index-scaled IEM with NFW-c profile are already excluded by direct detection experiments. This latter model is consistent with vanishing coupling to quarks, and thus is unlikely to be excluded by searches at the LHC.

VI. SUMMARY

The excess of ~GeV γ-rays from the direction of the GC is an indication that there is something in the γ-ray sky beyond our current knowledge. Whether this source ultimately proves to originate from DM annihilation or from a more conventional astrophysical source still remains to be determined, and is likely to require further experimental input. As part of this process, we have examined key aspects of the putative signal using the specialized IEMs, developed by the *Fermi*-LAT Collaboration [19]. Our goal in characterizing potential DM explanations is to explore the implications from complementary searches, which can rule out or favor a DM interpretation.

Our results illustrate the impact of interstellar emission modeling on the extracted characteristics of the excess and highlight the need for improved modeling to capture a more realistic range of possibilities. As far as the gross characteristics of the excess are concerned, we find an offset of ~0.5° of

the excess centroid from Sgr A* for all four IEMs considered. We further find no significant evidence that the tail of the excess has a different spatial morphology than the few GeV bump, with both high energy and low energy components favoring an NFW morphology compared to the other morphologies we have considered.

We also consider flexible and realistic particle physics models for DM interacting with up-type quarks, down-type quarks, and charged leptons, for two separate interaction types (pseudoscalar and vector) leading to s-wave annihilation. These theories are described by EFTs, valid when the momentum transfer is small compared to the masses of the particles mediating the interactions—to describe annihilation, this implies the mediators are heavier than the DM itself. We find that the choice of IEM has a large impact on the preferred DM mass, annihilation cross section, and primary annihilation channel. In particular, we identify regions with higher masses and annihilation predominantly into top quarks. Comparing the ML points in parameter space with direct and collider searches, we find that all of the vector models aside from one at DM mass ∼10 GeV and annihilating into leptons are ruled out by null results from the LUX experiment. The pseudoscalar models predict spin-dependent and velocity-dependent scattering with nuclei at a rate far below the current sensitivity, but in some cases within the grasp of future planned experiments. It would be interesting, but beyond the scope of this work, to extend our analysis beyond the EFT limit to the case of models where the DM can annihilate directly into the mediator particles themselves.

The GeV excess is a compelling hint that there is more to learn about the Galaxy. It is likely to take a combined effort of observation and interpretation to unravel its nature.

ACKNOWLEDGMENTS

The authors are pleased to acknowledge conversations with D. Finkbeiner, D. Hooper, M. Kaplinghat, T. Slatyer, and C. Weniger. The work of C. K. and S. M. is supported in part by Department of Energy Grant No. DE-SC0014431. The work of T. M. P. T. and P. T. is supported in part by National Science Foundation Grants No. PHY-1316792 and No. PHY-1620638. GALPROP development is partially funded via NASA Grants No. NNX09AC15G, No. NNX10AE78G, and No. NNX13AC47G.

[1] M. Ackermann *et al.* (Fermi-LAT Collaboration), Phys. Rev. D **89**, 042001 (2014).
[2] M. Ackermann *et al.* (Fermi-LAT Collaboration), Phys. Rev. Lett. **115**, 231301 (2015).
[3] A. Geringer-Sameth and S. M. Koushiappas, Phys. Rev. Lett. **107**, 241303 (2011).
[4] L. Goodenough and D. Hooper, arXiv:0910.2998.
[5] D. Hooper and L. Goodenough, Phys. Lett. B **697**, 412 (2011).
[6] D. Hooper and T. Linden, Phys. Rev. D **84**, 123005 (2011).
[7] K. N. Abazajian and M. Kaplinghat, Phys. Rev. D **86**, 083511 (2012); **87**, 129902(E) (2013).
[8] D. Hooper and T. R. Slatyer, Phys. Dark Univ. **2**, 118 (2013).
[9] C. Gordon and O. Macias, Phys. Rev. D **88**, 083521 (2013); **89**, 049901 (2014).
[10] W.-C. Huang, A. Urbano, and W. Xue, arXiv:1307.6862.
[11] T. Daylan, D. P. Finkbeiner, D. Hooper, T. Linden, S. K. N. Portillo, N. L. Rodd, and T. R. Slatyer, Phys. Dark Univ. **12**, 1 (2016).
[12] K. N. Abazajian, N. Canac, S. Horiuchi, and M. Kaplinghat, Phys. Rev. D **90**, 023526 (2014).
[13] B. Zhou, Y.-F. Liang, X. Huang, X. Li, Y.-Z. Fan, L. Feng, and J. Chang, Phys. Rev. D **91**, 123010 (2015).
[14] F. Calore, I. Cholis, and C. Weniger, J. Cosmol. Astropart. Phys. 03 (2015) 038.
[15] K. N. Abazajian, N. Canac, S. Horiuchi, M. Kaplinghat, and A. Kwa, J. Cosmol. Astropart. Phys. 07 (2015) 013.
[16] F. Calore, I. Cholis, C. McCabe, and C. Weniger, Phys. Rev. D **91**, 063003 (2015).
[17] X. Huang, T. Enlin, and M. Selig, J. Cosmol. Astropart. Phys. 04 (2016) 030.
[18] E. Carlson, T. Linden, and S. Profumo, Phys. Rev. D **94**, 063504 (2016).
[19] M. Ajello *et al.* (Fermi-LAT Collaboration), Astrophys. J. **819**, 44 (2016).
[20] D. Hooper, I. Cholis, T. Linden, J. Siegal-Gaskins, and T. Slatyer, Phys. Rev. D **88**, 083009 (2013).
[21] E. Carlson and S. Profumo, Phys. Rev. D **90**, 023015 (2014).
[22] J. Petrović, P. D. Serpico, and G. Zaharija, J. Cosmol. Astropart. Phys. 10 (2014) 052.
[23] I. Cholis, D. Hooper, and T. Linden, J. Cosmol. Astropart. Phys. 06 (2015) 043.
[24] I. Cholis, C. Evoli, F. Calore, T. Linden, C. Weniger, and D. Hooper, J. Cosmol. Astropart. Phys. 12 (2015) 005.
[25] O. Macias, C. Gordon, R. M. Crocker, B. Coleman, D. Paterson, S. Horiuchi, and M. Pohl, arXiv:1611.06644.
[26] S. K. Lee, M. Lisanti, and B. R. Safdi, J. Cosmol. Astropart. Phys. 05 (2015) 056.
[27] R. Bartels, S. Krishnamurthy, and C. Weniger, Phys. Rev. Lett. **116**, 051102 (2016).
[28] S. K. Lee, M. Lisanti, B. R. Safdi, T. R. Slatyer, and W. Xue, Phys. Rev. Lett. **116**, 051103 (2016).
[29] S. D. McDermott, P. J. Fox, I. Cholis, and S. K. Lee, J. Cosmol. Astropart. Phys. 07 (2016) 045.

[30] S. Horiuchi, M. Kaplinghat, and A. Kwa, J. Cosmol. Astropart. Phys. 11 (2016) 053.
[31] M. Ackermann *et al.* (Fermi-LAT Collaboration), Astrophys. J. Suppl. Ser. **203**, 4 (2012).
[32] W. Atwood *et al.* (Fermi-LAT Collaboration), arXiv: 1303.3514.
[33] C. Weniger (private communication).
[34] J. R. Mattox *et al.*, Astrophys. J. **461**, 396 (1996).
[35] J. F. Navarro, C. S. Frenk, and S. D. M. White, Astrophys. J. **490**, 493 (1997).
[36] J. Diemand, M. Zemp, B. Moore, J. Stadel, and M. Carollo, Mon. Not. R. Astron. Soc. **364**, 665 (2005).
[37] M. Kuhlen, J. Guedes, A. Pillepich, P. Madau, and L. Mayer, Astrophys. J. **765**, 10 (2013).
[38] D. Lena, A. Robinson, A. Marconi, D. J. Axon, A. Capetti, D. Merritt, and D. Batcheldor, Astrophys. J. **795**, 146 (2014).
[39] T. Linden, N. L. Rodd, B. R. Safdi, and T. R. Slatyer, Phys. Rev. D **94**, 103013 (2016).
[40] M. Beltran, D. Hooper, E. W. Kolb, and Z. C. Krusberg, Phys. Rev. D **80**, 043509 (2009).
[41] H. Zhang, Q.-H. Cao, C.-R. Chen, and C. S. Li, J. High Energy Phys. 08 (2011) 018.
[42] M. Beltran, D. Hooper, E. W. Kolb, Z. A. C. Krusberg, and T. M. P. Tait, J. High Energy Phys. 09 (2010) 037.
[43] J. Goodman, M. Ibe, A. Rajaraman, W. Shepherd, T. M. P. Tait, and H.-B. Yu, Phys. Rev. D **82**, 116010 (2010).
[44] J. Goodman, M. Ibe, A. Rajaraman, W. Shepherd, T. M. P. Tait, and H.-B. Yu, Nucl. Phys. **B844**, 55 (2011).
[45] J. Kumar and D. Marfatia, Phys. Rev. D **88**, 014035 (2013).
[46] A. Alves, S. Profumo, F. S. Queiroz, and W. Shepherd, Phys. Rev. D **90**, 115003 (2014).
[47] S. Liem, G. Bertone, F. Calore, R. Ruiz de Austri, T. M. P. Tait, R. Trotta, and C. Weniger, J. High Energy Phys. 09 (2016) 077.
[48] C. Boehm, M. J. Dolan, C. McCabe, M. Spannowsky, and C. J. Wallace, J. Cosmol. Astropart. Phys. 05 (2014) 009.
[49] M. Abdullah, A. DiFranzo, A. Rajaraman, T. M. P. Tait, P. Tanedo, and A. M. Wijangco, Phys. Rev. D **90**, 035004 (2014).
[50] A. Martin, J. Shelton, and J. Unwin, Phys. Rev. D **90**, 103513 (2014).
[51] A. Berlin, P. Gratia, D. Hooper, and S. D. McDermott, Phys. Rev. D **90**, 015032 (2014).
[52] C. Balzs and T. Li, Phys. Rev. D **90**, 055026 (2014).
[53] P. Ko and Y. Tang, J. Cosmol. Astropart. Phys. 01 (2015) 023.
[54] E. C. F. S. Fortes, V. Pleitez, and F. W. Stecker, Astropart. Phys. **74**, 87 (2016).
[55] L. M. Carpenter, R. Colburn, J. Goodman, and T. Linden, Phys. Rev. D **94**, 055027 (2016).
[56] M. Escudero, A. Berlin, D. Hooper, and M.-X. Lin, J. Cosmol. Astropart. Phys. 12 (2016) 029.
[57] G. D'Ambrosio, G. F. Giudice, G. Isidori, and A. Strumia, Nucl. Phys. **B645**, 155 (2002).
[58] M. Cirelli, G. Corcella, A. Hektor, G. Hutsi, M. Kadastik, P. Panci, M. Raidal, F. Sala, and A. Strumia, J. Cosmol. Astropart. Phys. 03 (2011) 051; 10 (2012) E01.
[59] T. Sjostrand, S. Mrenna, and P. Z. Skands, Comput. Phys. Commun. **178**, 852 (2008).
[60] P. Agrawal, B. Batell, P. J. Fox, and R. Harnik, J. Cosmol. Astropart. Phys. 05 (2015) 011.
[61] C. Balzs and T. Li, J. Cosmol. Astropart. Phys. 02 (2017) 037.
[62] G. Steigman, B. Dasgupta, and J. F. Beacom, Phys. Rev. D **86**, 023506 (2012).
[63] M. Cirelli, P. D. Serpico, and G. Zaharijas, J. Cosmol. Astropart. Phys. 11 (2013) 035.
[64] T. Lacroix, C. Boehm, and J. Silk, Phys. Rev. D **90**, 043508 (2014).
[65] A. Geringer-Sameth, M. G. Walker, S. M. Koushiappas, S. E. Koposov, V. Belokurov, G. Torrealba, and N. W. Evans, Phys. Rev. Lett. **115**, 081101 (2015).
[66] K. Hayashi, K. Ichikawa, S. Matsumoto, M. Ibe, M. N. Ishigaki, and H. Sugai, Mon. Not. R. Astron. Soc. **461**, 2914 (2016).
[67] N. Bernal, L. Necib, and T. R. Slatyer, J. Cosmol. Astropart. Phys. 12 (2016) 030.
[68] K. Ichikawa, M. N. Ishigaki, S. Matsumoto, M. Ibe, H. Sugai, and K. Hayashi, arXiv:1608.01749.
[69] N. Klop, F. Zandanel, K. Hayashi, and S. Ando, arXiv: 1609.03509.
[70] J. Kopp, J. Liu, T. R. Slatyer, X.-P. Wang, and W. Xue, J. High Energy Phys. 12 (2016) 033.
[71] K. N. Abazajian and R. E. Keeley, Phys. Rev. D **93**, 083514 (2016).
[72] O. Adriani *et al.* (PAMELA Collaboration), Nature (London) **458**, 607 (2009).
[73] M. Aguilar *et al.* (AMS Collaboration), Phys. Rev. Lett. **110**, 141102 (2013).
[74] L. Bergstrom, T. Bringmann, I. Cholis, D. Hooper, and C. Weniger, Phys. Rev. Lett. **111**, 171101 (2013).
[75] A. Cuoco, M. Krmer, and M. Korsmeier, arXiv: 1610.03071.
[76] M.-Y. Cui, Q. Yuan, Y.-L. S. Tsai, and Y.-Z. Fan, 2016), arXiv:1610.03840.
[77] M. Aguilar *et al.* (AMS Collaboration), Phys. Rev. Lett. **117**, 091103 (2016).
[78] G. Giesen, M. Boudaud, Y. Gnolini, V. Poulin, M. Cirelli, P. Salati, and P. D. Serpico, J. Cosmol. Astropart. Phys. 09 (2015) 023.
[79] M. G. Aartsen *et al.* (IceCube Collaboration), Eur. Phys. J. C **77**, 146 (2017).
[80] A. L. Fitzpatrick, W. Haxton, E. Katz, N. Lubbers, and Y. Xu, J. Cosmol. Astropart. Phys. 02 (2013) 004.
[81] N. Anand, A. L. Fitzpatrick, and W. C. Haxton, Phys. Rev. C **89**, 065501 (2014).
[82] M. Cirelli, E. Del Nobile, and P. Panci, J. Cosmol. Astropart. Phys. 10 (2013) 019.
[83] M. I. Gresham and K. M. Zurek, Phys. Rev. D **89**, 123521 (2014).
[84] D. S. Akerib *et al.*, arXiv:1608.07648.
[85] J. Aalbers *et al.* (DARWIN Collaboration), J. Cosmol. Astropart. Phys. 11 (2016) 017.
[86] J. Billard, L. Strigari, and E. Figueroa-Feliciano, Phys. Rev. D **89**, 023524 (2014).
[87] G. Aad *et al.* (ATLAS Collaboration), J. High Energy Phys. 04 (2013) 075.
[88] V. Khachatryan *et al.* (CMS Collaboration), Eur. Phys. J. C **75**, 235 (2015).
[89] J. Fan, S. M. Koushiappas, and G. Landsberg, J. High Energy Phys. 01 (2016) 111.